Malaysian Journal of Chemistry, 2026, Vol. 28(1), 442-452
(Special Issue: *12th International Conference of the College of Science & 3rd Conference of Chemistry Department 2025*)

Integration of NiS–SrO Nanostructures in Tartrazine-Dye-Sensitized Solar Cells: Photolytic Fabrication and Efficiency Enhancement

Sara Younis Abdullah and Ahmed Mahdi Rheima*
Chemistry Department, Mustansiriyah University, College of Science, Baghdad,10011, Iraq
*Corresponding author (email: ahmed.rheima@gmail.com)

In this work, NiS, SrO, and their hybrid NiS–SrO nanostructures were fabricated via photolysis and subsequently used as photo-anodes in dye-sensitized solar cells (DSSCs). The electrolyte depended on an iodide/triiodide redox pair, the counter electrode was constructed from a CNT–FeS nanocomposite, and the photo-sensitizer was tartrazine yellow dye. A structural analysis reveals that the resulting nanostructures possess morphological features particularly advantageous for intense light absorption and rapid charge transport, with crystallites in the 16–21 nm range. According to photovoltaic tests, the NiS-based cell pushed the conversion efficiency up to roughly 2.9%, whereas the SrO-based cell just scraped a 2.25% conversion efficiency due to its conductivity. The binary between NiS and SrO is responsible for the remarkable increase in efficiency of the NiS–SrO nanocomposite device, which reached 3.25%. While SrO works as an electron blocking barrier to prevent charge recombination at the electrode–electrolyte interface, the NiS phase acts as a courier, speeding up charge transport and snagging more dye molecules. The information presented in this work highlights how the NiS–SrO nanocomposite is gradually establishing a position as a photo-anode material for constructing stable DSSCs.

Keywords: Photolysis method, Tartrazine yellow dye, photo-sensitizer, dye-sensitized solar cells (DSSCs), hybrid NiS–SrO nanostructures

Received: October 2025; Accepted: October 2025

Solar energy is one of the substitutes for the antiquated fossil fuel paradigm that provides a plentiful, sustainable, and ecologically friendly power source [1]. Sunshine from natural gas or coal is almost limitless, unlike the finite oil supplies. It can be utilized in several international settings [2]. Dye-sensitized solar cells (DSSCs), a new generation of photovoltaic cells with low cost, ease of fabrication, and great potential for converting solar energy into electrical energy with acceptable efficiency, are among the most promising innovations in this field. Photovoltaic cells, sometimes referred to as cells, continue to dominate the variety of solar-capture systems because of their capacity to use the photovoltaic effect to convert sunlight into energy [3]. The mechanism of electron transfer between the valence and conduction bands in semiconductors has led to new horizons in clean energy generation across various fields. However, conventional photovoltaic modules face challenges in achieving these gains, with persistent drawbacks: their inefficiency, high manufacturing costs, and some drawbacks, including stability issues, that hinder their wider market penetration [4]. In the same context, nanotechnology has emerged as a major supporter in developing and enhancing the efficiency of solar cells [5]. Due to their size and distinctive properties, nanomaterials have proven their ability to enhance light efficiency, improve charge separation, and accelerate electron transfer in solar devices [6]. Because they are tunable, their band gap can be easily tuned with the spectrum, and their apparent surface-to-volume ratio allows for countless points to which photons can attach [7]. Furthermore, the high flexibility of nanomaterials makes them suitable for use in a wide range of solar technologies, such as dye-sensitized solar cells (DSSCs), thin films, and rapidly scaling perovskite-based devices [8]. This field has demonstrated high efficiency, with nickel sulfide (NiS) attracting the attention of researchers for its combination of efficiency and ease of use [9]. Due to its strength and excellent electrical conductivity, nickel sulfide provides an alternative to platinum, an anti-polarizing material, and is very useful in dye-sensitized solar cells (DSSCs) [10]. Furthermore, because of its semiconductor qualities, nickel sulfide (NiS) can be deposited as a layer onto thin-film cells. It is more attractive for widespread solar energy deployment because of its ease of manufacturing and ability to facilitate charge transfer connections [11]. Strontium oxide (SrO) is one of the most promising options in state-of-the-art photovoltaic research. When incorporated into electronics, strontium oxide's wide band gap and activity result in improved light capture. It has been demonstrated that strontium oxide nanoparticles improve solar cell stability by lowering recombination losses and giving the layers more flexibility [12]. Moreover, SrO-based composites display pronounced activity, making them attractive for a variety of energy-conversion and processing

---

†Paper presented at the 12th International Conference of the College of Science & 3rd Conference of Chemistry Dept. 2025

applications [13]. This feature makes them ideal for environmentally friendly modules that try to satisfy the growing demand for electricity worldwide. Carbon nanotubes (CNTs) give photovoltaic technology a competitive edge. CNTs are practically intended to be conductors for cells because of their extraordinary ability to whisk electrons across, as well as their shape and expansive surface [14]. Researchers have occasionally experimented with hybridizing these nanotubes with sulfide species, with iron sulfide (FeS) emerging as a promising option. A CNT-FeS nanocomposite that exhibits a noticeable effect is created when the conductivity of the nanotubes and the redox vigor of FeS are married [15, 16]. Because of its special capacity to blend reactivity and absorption, CNT-FeS can be used to remove dyes and other impurities from solutions in addition to powering solar cells, demonstrating its broad range of applications [17]. Consequently, embedding NiS, SrO, and CNT-FeS composites into device architectures is poised to boost power-conversion efficiency, fortify stability, and lift photovoltaic performance [18]. By capturing sunlight, streamlining charge movement, and slashing material and production expenses, these additives directly tackle many of the shortcomings that plague solar cells. Beyond power generation, their adaptable nature, in adsorption and catalysis, also earmarks them as tools for technological advances and environmental safeguards [19–21]. The purpose of the manufacture, characterization, and photovoltaic efficacy of advanced nanotechnology is examined in this article, underscoring their potential as highly efficient alternatives to future solar energy systems. The work illustrates how nanotechnology is impacting the energy industry and paving the way for a more sustainable future by fusing materials science with renewable energy engineering.

EXPERIMENTAL

Synthesis of NiS Nanostructures

Nickel sulfide (NiS) nanoparticles have been synthesized using a photolysis method. First, 50 ml of 20 mM Nickel Nitrate solution as a formula [Ni(NO3)2] was prepared, followed by 50 ml of 20 mM Urea solution (drop by drop). The resulting mixture was continuously stirred for 15 minutes using a magnetic stirrer to ensure continuity. Then the solution was transferred to a photolysis cell and exposed to radiation for 30 minutes (by a 125 W medium-pressure mercury lamp, delivering maximum intensity at a wavelength of 365 nm). After that, 50 ml of 0.02 M sodium sulfide solution (Na2S) was added to the mixture, resulting in the formation of a black precipitate that indicated the presence of (NiS) nanoparticles. It was separated by filtration, washed several times with deionized water to remove impurities, and then dried in an oven for 3h at 95 °C.

Synthesis of SrO Nanostructures

Strontium oxide (SrO) nanoparticles were synthesized using a photolysis method. Originally, 3 grams of SrCO3 were placed in a reaction vessel, and 100 ml of deionized water was added, stirred for 15 minutes to ensure proper dispersion. Then 50 ml of 0.1 M hydrochloric acid (HCl) was added to the mixture, followed by a dropwise addition of 50 ml of 0.03M urea solution at a controlled rate of one drop per second under continuous magnetic stirring. The resulting solution was transferred to a photolysis cell and exposed to radiation for 30 min. The radiation caused precipitation to form. To obtain (SrO) nanoparticles, the precipitate was collected, repeatedly washed with deionized water, dried, and calcined to 400 °C.

Synthesis of Binary NiS –SrO Nanostructures

Binary NiS –SrO Nanoparticles were synthesized by the same method (photolysis method). Originally, 1 gram of strontium oxide (SrO) was dispersed in 100 ml of deionized water, stirred continually to ensure a uniform suspension. Then, 100 mL of 0.02 M nickel nitrate [$Ni(NO_3)_2$] solution was added dropwise to the suspension. The resulting mixture was transferred to a photochemical cell and exposed to radiation for 30 minutes. After irradiation, 0.1 M sodium sulfide (Na_2S) was added to the mixture, leading to the formation of a black precipitate. The precipitate was collected, thoroughly washed several times with deionized water to remove any residual impurities, and then dried in an oven at 90 °C for 5 hr to obtain binary (SrO–NiS) nanoparticles.

Fabrication of Dye-sensitized Solar Cells

Preparation of Electrolyte Solution

The iodide/triiodide (I^-/I 3^-) Redox pairs are the most used in dye-sensitized solar cells (DSSC). In this study, the electrolyte solution was prepared by dissolving 1.66g of potassium iodide in 20 mL of distilled water to achieve a 0.5 M solution. Then 0.12 g of iodine was added to the solution, which was then mixed for 10 minutes to ensure complete dissolution and homogeneity [22].

Making Dye-sensitized Solar Cells

Fabrication of Dye-Sensitized Solar Cells with NiS as the Catalyst, the Indium Doped Tin Oxide (ITO) coated glass (resistance 8 ohms, transmittance 83%) was cleaned thoroughly by ultrasonic washing with acetone, ethanol, and distilled water to remove impurities, then dried using compressed air. A colloidal solution of NiS nanoparticles was prepared by mixing iron oxide powder with ethanol. The photoanode was created by depositing this colloidal solution onto the conductive side of the cleaned glass using a dropper to ensure uniform coverage. The coated glass was then annealed at 200°C for 30 minutes in air. After cooling, the NiS nanoparticle electrode was immersed in a 0.5 mM Rhodamine 6G dye solution for 24 hours at room temperature to facilitate dye adsorption. The counter electrode was coated with NiS nanoparticles using a thermal evaporation technique in a vacuum. Once both electrodes were prepared, they were assembled with the liquid electrolyte containing I^- / $I3^-$ redox couple. The electrolyte was allowed to penetrate the cell via capillary action. The assembled cell was secured using a binder clip to ensure stability. This NiS-based catalyst aims to enhance charge transfer and improve the efficiency of the dye-sensitized solar cell.

Characterization Instruments

The morphological features and particle size of the produced nanostructures were investigated with a technical Vega 3 SB Field emission scanning electron microscope (FE-SEM). Crystallographic analysis was performed using a Shimadzu XRD-6000 X-ray diffractometer to identify structural stages and estimate crystalline sizes. In addition, a fast voltage of 100 kV was used to operate the transmission electron microscope (TEM). Using a JEOL JEM-2100 to check the internal structure and detailed morphology of nanoparticles. The elemental composition and surface distribution of elements were evaluated using Energy-Dispersive X-ray spectroscopy (EDX), which was done with the JSM-6510LV system.

RESULTS AND DISCUSSION

Characterizations of SrO-NiS Nanostructures

The XRD pattern of the synthesized NiS nanostructures (Figure 1) reveals not only the characteristic reflections of NiS but also additional crystalline phases. Notably, a peak around 38.5° corresponds to the (200) plane of cubic NiO (JCPDS No. 47-1049), while a peak near 57.5° is attributed to the (511) plane of Ni_3S_2 (JCPDS No. 44-1418). Additionally, a minor reflection observed at approximately 66.2° is associated with the (220) plane of NiO. These supplementary peaks confirm the coexistence of secondary phases NiO and Ni_3S_2 alongside the primary NiS phase [23]. This phase mixture likely results from partial surface oxidation and variations in the NiS composition during the photochemical process. The broad peaks observed suggest a nanocrystalline structure, with the crystallite size estimated to be around 16.43 nm via the Scherrer equation, indicating nanoscale dimensions [24]. Importantly, the absence of unidentified diffraction signals suggests that the material predominantly comprises NiS, with minor contributions from NiO and Ni_3S_2, confirming the effectiveness of the photochemical synthesis route in producing crystalline nickel sulfide nanoparticles with controlled phase composition [25].

Regarding the SrO nanoparticles (Figure 2), their XRD pattern displays peaks corresponding to the (100), (110), (200), (111), (210), (211), (220), and (310) planes at 2θ values of 25.5°, 31.8°, 35.5°, 36.8°, 50.4°, 57.6°, 59.1°, and 75.1°, respectively. These peaks align well with standard JCPDS data (No: 06-0520, 01-1113, 37.5-0263, 01-073-0661), verifying the high crystallinity and successful formation of SrO as the dominant phase [26]. Additional weaker reflections, such as a peak at about 30.1°, are linked to the (110) plane of $Sr(OH)_2$, and a reflection around 43.1° corresponds to the (202) plane of $SrCO_3$. These arise from interactions with atmospheric moisture and CO_2, leading to hydroxide and carbonate formation [27]. Despite their presence, these secondary phases show much lower intensity compared to the main SrO peaks, reaffirming SrO as the primary crystalline component. The peak broadening indicates a nanocrystalline structure, with the average crystallite size calculated to be approximately 21.11 nm using the Scherrer equation, consistent with reported nanoscale SrO particles [28].

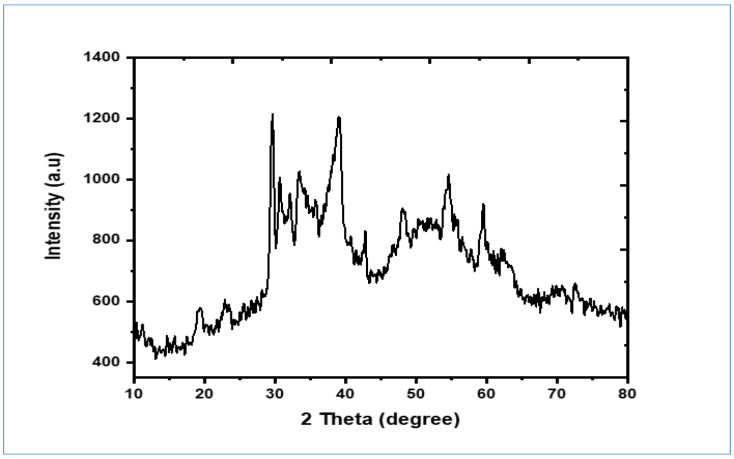

Figure 1. XRD pattern of the synthesis of NiS NPs.

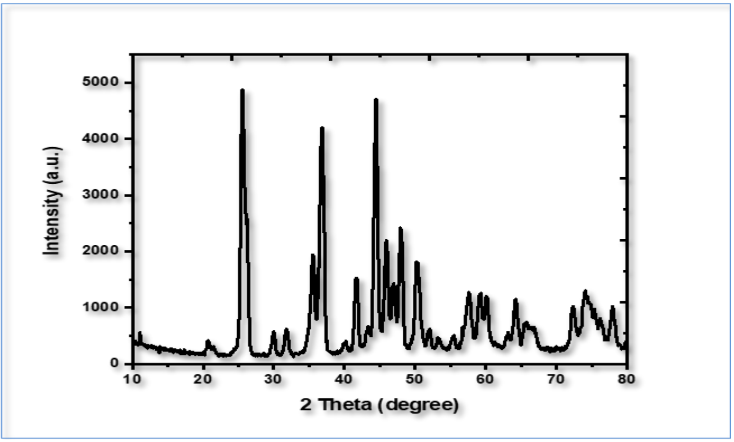

Figure 2. XRD pattern of the synthesis of SrO NPs.

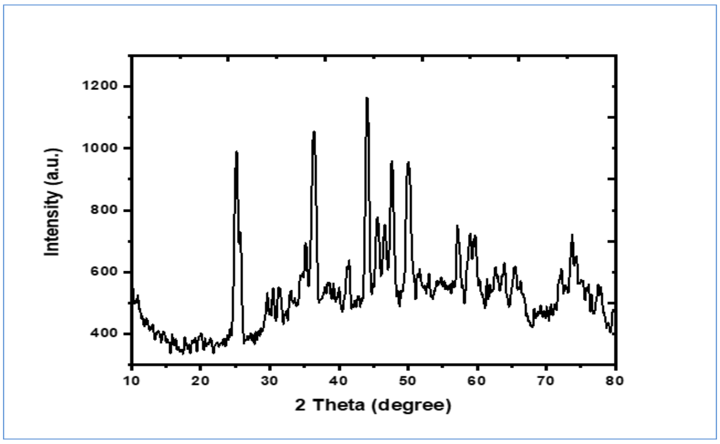

Figure 3. XRD pattern of the synthesis of SrO-NiS nanostructure.

For the SrO–NiS nanocomposite (Figure 3), the XRD pattern displays clear peaks associated with both SrO and NiS phases. Prominent SrO reflections are observed at 2θ ≈ 25.8°, 32.1°, 35.8°, 37.6°, 50.8°, 58.2°, 59.4°, and 75.8°, matching standard JCPDS references. Simultaneously, characteristic NiS peaks appear at 2θ ≈ 30.2°, 34.8°, 45.5°, 53.3°, and 62.4°, corresponding to hexagonal NiS [29]. Additional diffraction features between 35°–55° and 60°–70° suggest interactions and possible formation of mixed oxide–sulfide phases within the composite, likely induced by the photochemical synthesis process [30]. The average crystallite size of the nanocomposite, estimated via the Scherer equation, is approximately 18.7 nm, confirming its nanometer scale [31].

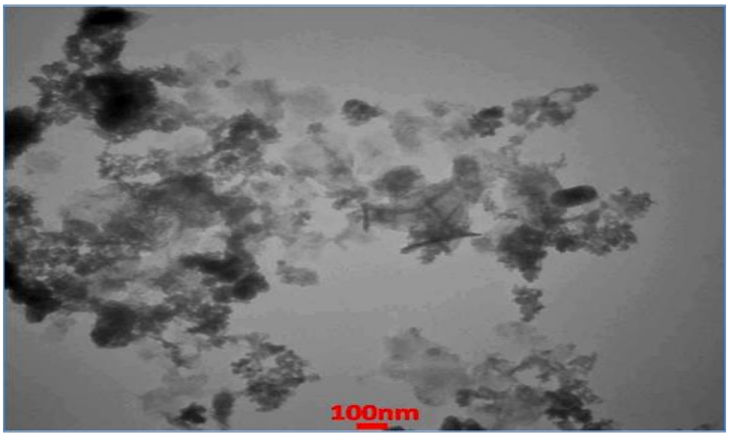

Figure 4. TEM images of the synthesis of NiS NPs.

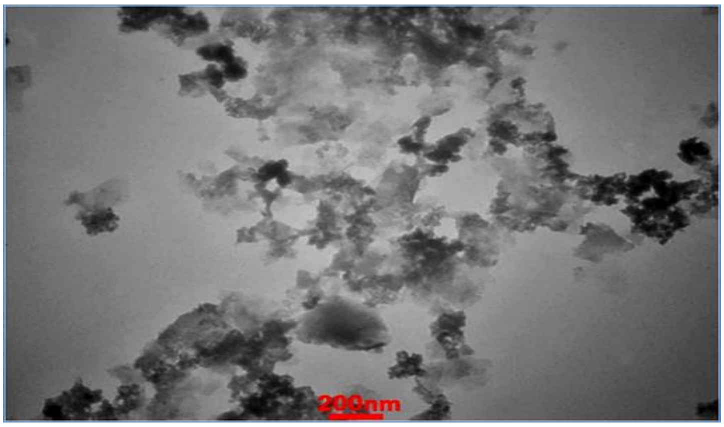

Figure 5. TEM images of the synthesis of SrO NPs.

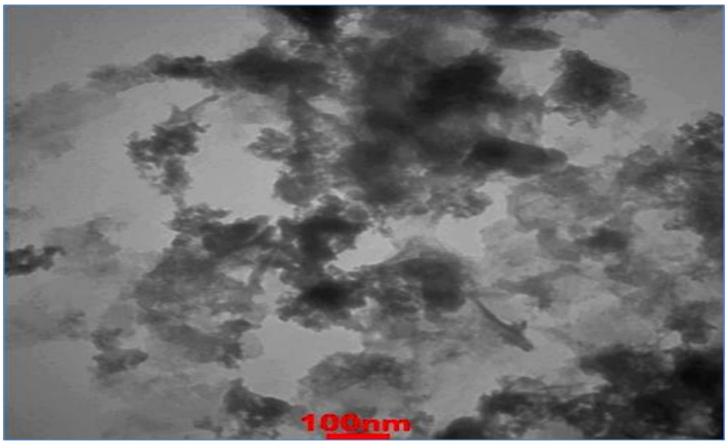

Figure 6. TEM images of the synthesis of SrO-NiS nanostructure.

The particle size and morphology of the synthesized nanomaterials were examined using Transmission Electron Microscopy (TEM). Average particle sizes were determined through random measurements from the TEM micrographs, as depicted in Figures 4, 5, and 6. The TEM images demonstrated that all synthesized nanomaterials possess a spherical morphology and are free from significant aggregation [32]. The use of urea as a surfactant, in combination with UV radiation, was crucial in producing well-dispersed nanoparticles with distinct boundaries. This synthesis method follows a bottom-up approach, beginning with the formation of Nano nuclei in the presence of surfactant under ultraviolet illumination, followed by particle growth until the desired size is attained [33]. Furthermore, the particle sizes, estimated randomly from the TEM images, revealed averages of approximately 25 nm for NiS nanoparticles, 28 nm for SrO nanoparticles, and about 22 nm for the NiS–SrO nanocomposite. This approach facilitated the formation of uniform, small-sized nanoparticles [34]. All particles measured were below 100 nm, classifying them as zero-dimensional (0D) nanomaterials. Additionally, the particle sizes derived from TEM analyses showed good consistency with the crystalline sizes calculated from the Debye–Scherrer equation based on XRD line broadening measurements [35].

FE-SEM has been utilized to examine the size distribution and morphology of the synthesized nanomaterials, as depicted in Figure 7, which shows a rough, irregular surface with prominent agglomerations, indicating high surface activity [36]. Conversely, Figure 8 exhibits a structure composed of short, intertwined particles, which results in a less rough surface but with a certain degree of structural complexity [37]. While distinct pores within the particles are not evident, their arrangement suggests the presence of voids, along with more organized agglomerations. Figure (9) presents a hybrid structure that combines features from Figures (7) and (8), implying that the material may exhibit electronic or catalytic properties due to the overlap and integration of these two constituent structures [38].

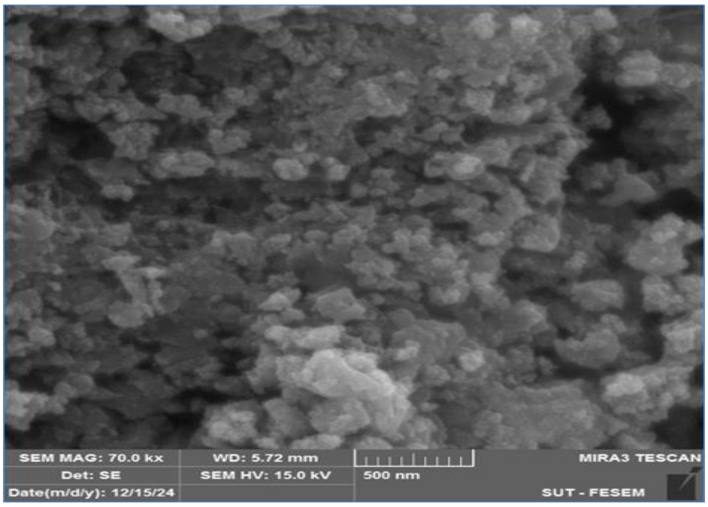

Figure 7. FE-SEM images of the synthesis of NiS NPs.

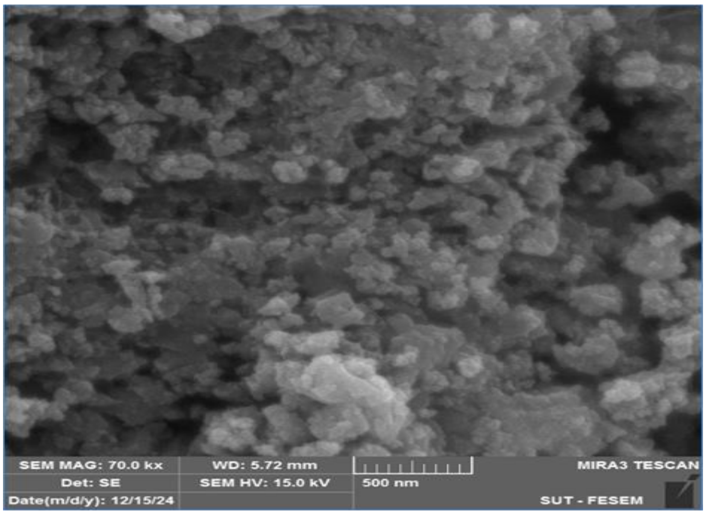

Figure 8. FE-SEM images of the synthesis of SrO NPs.

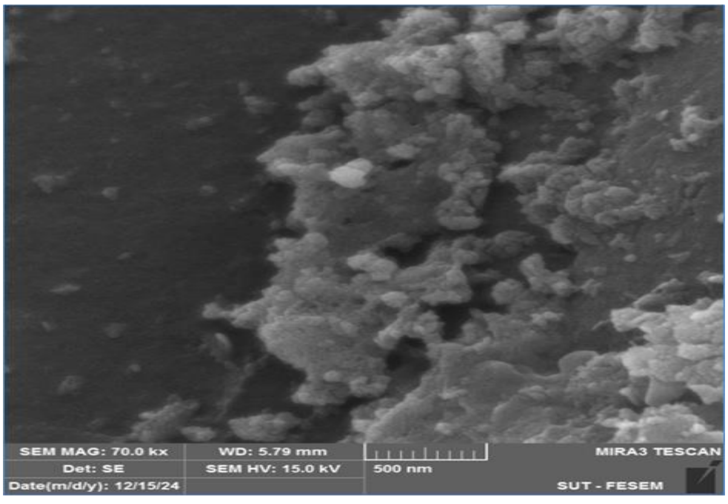

Figure 9. FE-SEM images the synthesis of SrO-NiS nanostructure.

EDX analysis was utilized to determine the chemical composition of three synthesized nanostructures, as illustrated in Figures 10, 11, and 12. The results indicated that the nickel-based nanoparticles primarily consist of nickel and sulfur elements, whereas the strontium oxide samples contain oxygen and strontium [39]. The third sample (SrO–NiS) comprises nickel, sulfur, oxygen, and strontium. The fourth sample predominantly contains carbon, while the fifth sample includes iron in the form of FeS alongside carbon. In addition to the expected main elements, minor peaks were observed, corresponding to trace amounts of other elements. These minor peaks may be attributed to factors such as the purity of the water used, sample preparation procedures, or residual impurities from starting materials [40]. Nonetheless, their concentrations are very low and do not significantly impact the overall composition or properties of the nanostructures. During EDX analysis, an electron beam is directed at the sample, causing the emission of characteristic X-rays [41]. Atoms in their ground state have specific electron energy levels or shells linked to the nucleus. When an inner-shell electron is ejected by the incident electron beam, an electron from an outer shell fills the vacancy, releasing excess energy in the form of characteristic X-ray photons unique to each element [42].

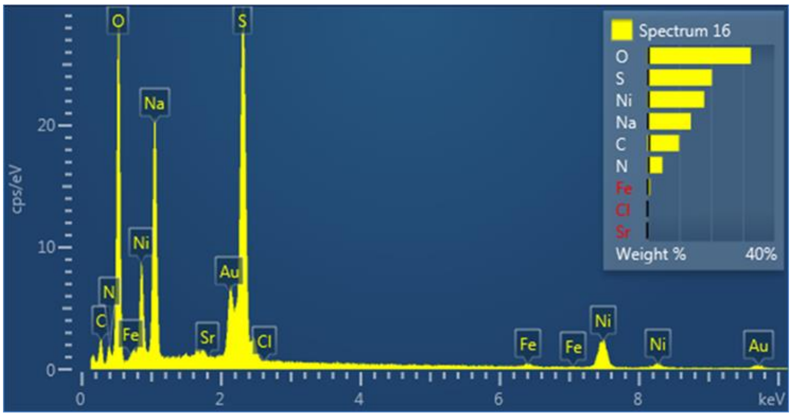

Figure 10. EDX spectrum of the Synthesis of NiS NPs.

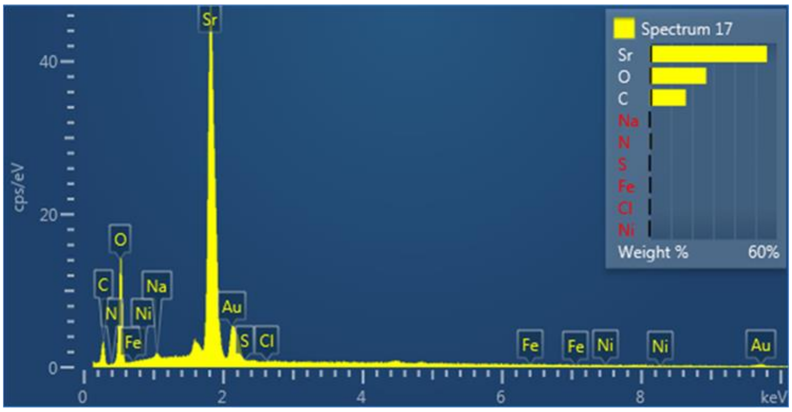

Figure 11. EDX spectrum of the Synthesis of SrO NPs.

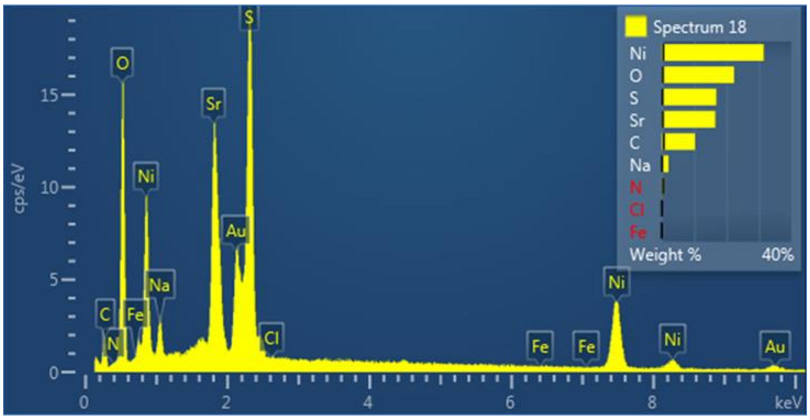

Figure 12. EDX Spectrum of the Synthesis of SrO-NiS nanostructure.

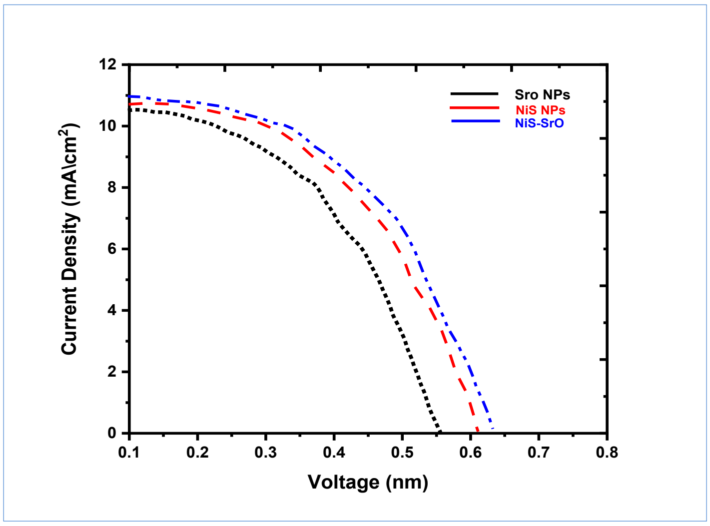

Figure 13. J–V characteristics of the fabricated DSSCs with different photo anodes.

Table 1. DSSC parameters of three photo-anodes: Nanostructures

Samples	Jsc (mA·cm^{-2})	Voc (V)	Vm (V)	Jm (mA·cm^{-2})	Pm (mW·cm^{-2})	FF	η (%)
SrO NPs	10.5	0.56	0.45	5.0	2.25	0.38	2.25
NiS NPs	10.8	0.60	0.48	6.0	2.88	0.44	2.9
NiS–SrO	11.0	0.63	0.50	6.5	3.25	0.47	3.25

Dye-sensitized Solar Cells (DSSCs)

The current density–voltage (J–V) characteristics of the fabricated dye-sensitized solar cells (DSSCs) with various photo anodes are shown in Figure 13. The photovoltaic parameters derived from these curves are summarized in Table 1. A digital multimeter (Pro Kit MT-1210) was used to measure both the open-circuit photo voltage (Voc) and the short-circuit photocurrent (Jsc) of the dye-sensitized solar cells (DSSCs). Illumination was provided by a solar simulator equipped with a halogen lamp, delivering a light intensity of (100 m W/cm²) to simulate standard sunlight conditions [43] [44]. The factor of DSSCs was determined by the following equations:

$$\eta = \boldsymbol{Pmax}/\text{Pin} = \text{voc} * \text{Jsc} * \text{FF}/\text{Pin} * 100 \qquad (1)$$

$$FF = V_{max} * J_{max} / V_{oc} * J_{sc} \qquad (2)$$

J_{sc} = short-circuit current density, V_{oc} = open-circuit photovoltaic voltage. FF= fill factor,

V_{max} and J_{max} denote the voltage and current density at maximum, respectively.

The device based on SrO nanoparticles exhibited the lowest performance, with a short-circuit current density (Jsc) of approximately 10.5 mA/cm^2, an open-circuit voltage (Voc) of around 0.56 V, a fill factor (FF) of about 0.38, and an overall efficiency of 2.25%. This relatively poor performance is mainly attributed to the low electrical conductivity of SrO, which increases the series resistance and hampers efficient charge transport [45]. On the other hand, the DSSC that used NiS nanoparticles showed better photovoltaic performance, with an efficiency of 2.9%, Jsc ≈ 10.8 mA/cm^2, Voc = 0.60 V, and FF = 0.44. NiS nanoparticles' increased conductivity and the existence of catalytic surface states, which promote electron transport and raise the fill factor, are the main causes of this improvement. It is considered chemically stable in addition to the narrow energy gap, which is what distinguishes this application [46]. The record-breaking efficiency of a sensitized cell that uses a NiS–SrO nanoparticle showed up as an open-circuit voltage of 0.63 V, a fill factor hovering around 0.47, a net efficiency of 3.25 percent, and a short-circuit density of 11.0 mA cm^{-2}. The two elements work together to provide this performance boost: NiS builds a charge-transport channel and provides docking sites for the dye, while SrO generates a blocking layer that limits electron recombination at the photo-anode/electrolyte interface. Overall, the hybrid photo-anode's performance was significantly higher than the meager yields of simpler arrangements, as it not only produced a denser photocurrent but also an improved open-circuit voltage. This result supports the idea that specially designed nanostructures, in this case NiS–SrO nanoparticles, offer a way to increase DSSC efficiencies over the limit defined by photo-anodes [47].

CONCLUSION

This study demonstrates that when utilized as the photo-anode in dye-sensitized solar cells (DSSCs), binary NiS–SrO nanostructures produced by a UV-assisted method provide superior photo-voltaic performance. The synergistic interaction of NiS and SrO greatly boosts device efficiency by increasing electron transport, lowering recombination charge, and enhancing dye-adsorption capacity. With a power conversion efficiency of 3.25%, the DSSC made from a blend of NiS and SrO NPs outperformed the NiS and SrO cells among all the samples analyzed. This illustrates how the NiS–SrO nanocomposite is a cost-effective photo-anode for the creation of solar energy conversion systems by mixing a metal oxide with a semiconducting sulfide to enhance stability and optimize charge transport.

REFERENCES

1. Asuni, O. H., Mahmud, M. D., Adesina, O. J., Matthew, U. O., Odubola, O. A. & Oyedemi, O. A. (2025). Advancing Renewable Energy Technology in an Emerging Zero-Carbon Society: Opportunities for Green Economy Sustainability. In Advanced Computation Solutions for Energy Efficiency. *IGI Global Scientific Publishing*, 37–68.

2. Al-Enizi, A. M., Al-Othman, A. M., Al-Askar, A. A., Al-Otaibi, F. M. & Habib, M. A. (2021) Green synthesis of nanomaterials for wastewater treatment: A review. *Chemosphere*, **282**, 131067.

3. Ansari, S. A., Al-Azizi, M. A., Al-Shahrani, F. A., Al-Qahtani, A. M. & Al-Amri, K. M. (2020) Emerging nanotechnologies for sustainable water treatment. *Nano Today*, **35**, 100985.

4. El-Moselhy, K., Al-Zahrani, A., Mansour, M. H., Shaban, S. A. & El-Sayed, Y. M. (2021) Photo-catalytic degradation of dyes using nanomaterials: Recent progress. *Environmental Chemistry Letters*, **19**, 1735–1756.

5. Ghaedi, M., Ansari, A., Tavallali, H. & Keshavarz, M. (2023) Functionalized nanomaterials for removal of toxic dyes from wastewater: A comprehensive review. *Journal of Cleaner Production*, **391**, 135085.

6. Kaur, A., Sharma, R., Singh, J., Kumar, V. & Mehta, S. (2021) Role of nanomaterials in wastewater remediation: Recent developments. *Materials Today Sustainability*, **14**, 100109.

7. Liu, Y., Wang, H., Zhang, L., Chen, X. & Zhao, J. (2022) Recent advances in nanotechnology for removing organic dyes from water. *Nanomaterials*, **12(14)**, 2459.

8. Mousavi, S. M., Hashemi, S. A., Bahrani, S. & Omidifar, N. (2021) Photocatalytic and adsorptive removal of water pollutants using nanostructured materials: A review. *Environmental Research*, **198**, 110796.

9. Nagpure, A., Kumar, R., Mishra, S. & Pandey, A. (2020) Eco-friendly nanomaterials for wastewater treatment: A review. *Environmental Chemistry Letters*, **18(3)**, 2219–2233.

10. Pant, D., Singh, R., Kumar, M. & Jain, P. (2022) Sustainable nanotechnology-enabled water treatment: A review. *Environmental Science & Technology*, **56(7)**, 4229–4244.

11. Razzak, S. A., Hossain, M. M., Lucky, R. A. & DeLasa, H. (2019) Application of nanotechnology in the removal of dyes from water: A review. *Environmental Chemistry Letters*, **17**, 955–974.

12. Salem, N., Abdelrahman, E. A., Fouda, M. M. & Abo-Elmagd, A. (2021) Advances in green synthesis of nanomaterials for environmental applications. *Journal of Environmental Management,* **280**, 111801.

13. Shah, A., Ahmad, N., Khan, A. & Sabir, S. (2020) Nanocomposite materials for wastewater treatment: A review. *Environmental Science: Nano*, **7(2)**, 489–502.

14. Singh, P., Verma, R., Gupta, A. & Sharma, S. (2023) Nanomaterials for removal of synthetic dyes: Recent advances and prospects. *Environmental Pollution*, **308**, 119580.

15. Khraisheh, M., Elhenawy, S., AlMomani, F., Al-Ghouti, M., Hassan, M. K. & Hameed, B. H. (2021) Recent progress on nanomaterial-based membranes for water treatment. *Membranes*, **11(12)**, 995.

16. Zhang, X., Li, Y., Wang, Z., Liu, H. & Chen, J. (2022) Sustainable nanotechnologies for organic dye removal: A review. *Environmental Research*, **204**, 111973.

17. Aftab, S., Khan, M., Ali, R. and Ahmed, N. (2025) Advancements in nanomaterials for solar energy harvesting. *Journal of Environmental Chemical Engineering*, **15(4)**, 105059.

18. Courel, M., Martínez, E., González, A. and López, J. (2025) State-of-the-Art nanomaterials for solar cells. *Nanomaterials*, **15(7)**, 508.

19. Farajollahi, A., Rezaei, S., Moradi, H. and Zhang, Y. (2025) Nanotechnology in solar energy: From active systems to advanced solar cells. *Frontiers in Energy Research*, **13**, 1560718.

20. Elezz, M. A., Hassan, W., Ibrahim, A. and Salem, N. (2025) Functional nanomaterials for energy and environmental applications: A comprehensive review. *Journal of Hazardous Materials Advances*, **5**, 100519.

21. Bhagya, N. P., Reddy, K. J., Kumar, V. and Prasad, B. (2025) Eco-friendly fabrication of SrO nanoparticles via Pongamia: Structural, optical, and application properties. *Ceramics International*, **51(12)**, 2265–2278.

22. Li, A. M., Zavalij, P. Y., Omenya, F., Li, X. and Wang, C. (2025) Salt-in-presalt electrolyte solutions for high-potential non-aqueous sodium metal batteries. *Nature Nanotechnology*, **20(3)**, 388–396.

23. Tai, H., Shi, J., Xu, D., Liang, K., Wang, X., Shi, L., and Liu, Z. (2024) Towards enhancing the performance of super capacitors: nanostructure engineering and optimal controlling crystal phase of NiS/Ni_3S_4 from metal-organic frameworks precursor. *Journal of Energy Storage*, **94**, 112397.

24. Gayathri, V., Ragavendran, V., Rajamanickam, N., Mayandi, J. and Nithiananthi, P. (2023) Mixed phase nanoarchitectonics of NiS@SnS@$Ni_3Sn_2S_2$ as a tetra-functional catalyst for dye-sensitized solar cells, super capacitors, and water splitting applications. *Journal of Energy Storage*, **70**, 107952.

25. Wang, X., Chen, H., Liu, L., Geng, L., Zhao, J., Wang, Y. and Bao, X. (2025) Preparation of NiO nanocrystals with different morphologies and their supercapacitive performance. *Chemical Physics*, **593**, 112637.

26. Elfadl, A. A., Bashal, A. H., Habeeb, T. H., Khalafalla, M. A., Alkayal, N. S. and Khalil, K. D. (2023) Preparation, characterization, dielectric properties, and AC conductivity of chitosan stabilized metallic oxides CoO and SrO: Experiments and tight binding calculations. *Polymers*, **15(20)**, 4132.

27. Anandhakumari, G., Jayabal, P., Jagadesan, A., Saravanakumar, M., Sambasivam, S., Alam, M. M. and Amanullah, M. (2024) Synergistic effect of strontium oxide–titanium oxide nanocomposites for photocatalytic degradation of malachite green dye. *Journal of Materials Science: Materials in Electronics*, **35(26)**, 1742.

28. Adimule, V., Keri, R., Rajendrachari, S., Kendrekar, P. and Kulkarni, C. V. (2023) Highly photo-luminescent and wide band gap insulating metal hybrid nanoparticles array of samarium-doped SrO:CoO: synthesis, characterizations, and sensor characteristics. *Journal of Materials Science: Materials in Electronics*, **34(5)**, 442.

29. Elfadl, A. A., Bashal, A. H., Habeeb, T. H., Khalafalla, M. A., Alkayal, N. S. and Khalil, K. D. (2023) Preparation, characterization, dielectric properties, and AC conductivity of chitosan stabilized metallic oxides CoO and SrO: Experiments and tight binding calculations. *Polymers*, **15(20)**, 4132.

30. Alshammari, A. H., Alshammari, K., Alotaibi, T., Alshammari, M., Alhassan, S. and Taha, T. A. M. (2023) In situ polycondensation synthesis of NiS-g-C_3N_4 nanocomposites for catalytic hydrogen generation from $NaBH_4$. *Nanomaterials*, **13(5)**, 938.

31. Almessiere, M. A., Slimani, Y., Algarou, N. A., Vakhitov, M. G., Klygach, D. S., Baykal, A. and Auwal, İ. A. (2022) Tuning the structure, magnetic, and high-frequency properties of Sc-doped $Sr_{0.5}Ba_{0.5}Sc_xFe_{12-x}O_{19}/NiFe_2O_4$ hard/soft nanocomposites. *Advanced Electronic Materials*, **8(2)**, 2101124.

32. Yin, L., Yang, J., Liu, L., Lu, B., Lyu, X., Cheng, Z. and An, X. (2025) Lignosulfonate as a versatile regulator for the mediated synthesis of Ag@AgCl nanocubes. *Nanoscale*, **17(5)**, 2451–2461.

33. Harish, V., Ansari, M. M., Tewari, D., Gaur, M., Yadav, A. B., García-Betancourt, M. L., and Barhoum, A. (2022) Nanoparticle and nanostructure synthesis and controlled growth methods. *Nanomaterials*, **12(18)**, 3226.

34. Polshettiwar, V. (2022) Dendritic fibrous nanosilica: discovery, synthesis, formation mechanism, catalysis, and CO_2 capture–conversion. *Accounts of Chemical Research*, **55(10)**, 1395–1410.

35. Coşkun, E., Kurşun, E., Yıldız, B., Aşkar, Y., Bahtiyar, D., Aydınol, M. K., and Çınar-Aygün, S. (2024) Size and morphology controlled polyol synthesis of $LiFePO_4$ nanoparticles with the addition of organic acid combinations. *Ceramics International*, **50(9)**, 15915–15930.

36. Kim, H., Han, J. and Han, T. Y. J. (2020) Machine vision-driven automatic recognition of particle size and morphology in SEM images. *Nanoscale*, **12(37)**, 19461–19469.

37. Polshettiwar, V. (2022) Dendritic fibrous nanosilica: discovery, synthesis, formation mechanism, catalysis, and CO_2 capture–conversion. *Accounts of Chemical Research*, **55(10)**, 1395–1410.

38. Cho, M. G., Sytwu, K., Dacosta, L. R., Groschner, C., Oh, M. H. and Scott, M. C. (2024). Size-resolved shape evolution in inorganic nanocrystals captured via high-throughput deep learning-driven statistical characterization. *ACS Nano*, **18(43)**, 29736–29747.

39. Sun, Y., Terrones, M. and Schaak, R. E. (2021) Colloidal nanostructures of transition-metal dichalcogenides. *Accounts of Chemical Research*, **54(6)**, 1517–1527.

40. Hussain, S., Farooq, N., Alkorbi, A. S., Alsaiari, R., Alhemiary, N. A., Wang, M. and Qiao, G. (2022) Polyhedral Co_3O_4@ZnO nanostructures as proficient photo-catalysts for vitiation of organic dyes from wastewater. *Journal of Molecular Liquids*, **362**, 119765.

41. Hafeez, M., Afyaz, S., Khalid, A., Ahmad, P., Khandaker, M. U. K., Sahibzada, M. U. K. and Idris, A. M. (2022) Synthesis of cobalt and sulfur-doped titanium dioxide photo-catalysts for environmental applications. *Journal of King Saud University – Science*, **34(4)**, 102028.

42. Al Zoubi, W., Putri, R. A. K., Abukhadra, M. R., Ko, Y. G. (2023) Recent experimental and theoretical advances in the design and science of high-entropy alloy nanoparticles. *Nano Energy*, **110**, 108362.

43. Kushwaha, A., Srivastava, D., Prakash, O., Kociok-Köhn, G., Gosavi, S. W., Chauhan, R. and Kumar, A. (2024) 1,1′-Bis-(diphenylphosphino) ferrocene appended d^8- and d^{10}-configuration based thiosquarates: the molecular and electronic configurational insights into their sensitization and co-sensitization properties for dye-sensitized solar cells. *Dalton Transactions*, **53(15)**, 6818–6829.

44. Kadhum, H. A., Salih, W. M. and Rheima, A. M. (2020) Improved PSi/c-Si and Ga/PSi/c-Si nanostructures dependent solar cell efficiency. *Applied Physics* A, **126(10)**, 1–5.

45. Savari, R., Rouhi, J., Fakhar, O., Kakooei, S., Pourzadeh, D., Jahanbakhsh, O. and Shojaei, S. (2021) Development of photo-anodes based on strontium-doped zinc oxide-reduced graphene oxide nanocomposites for improving the performance of dye-sensitized solar cells. *Ceramics International*, **47(22)**, 31927–31939.

46. Silambarasan, K., Archana, J., Athithya, S., Harish, S., Ganesh, R. S., Navaneethan, M. and Hayakawa, Y. (2020) Hierarchical NiO@NiS@graphene nanocomposite as a sustainable counter electrode for Pt-free dye-sensitized solar cells. *Applied Surface Science*, **501**, 144010.

47. Mirzaei, M. and Gholivand, M. B. (2024) P-doped NiS_2/Ni nanoheteroparticles embedded into N-doped carbon framework anchored on multi-walled carbon nanotubes as an efficient counter electrode for Pt-free dye-sensitized solar cells. *Materials Today Chemistry*, **35**, 101862.